Sensitivity of a one-line longshore shoreline change model to the mean wave direction

T. Chataigner, Marissa L. Yates, N. Le Dantec, M.D. Harley, K.D. Splinter, N. Goutal

Sensitivity of a one-line longshore shoreline change model to the mean wave direction

Chataigner T.[1], Yates M.L.[1], Le Dantec N.[3], Harley M.D.[4], Splinter K.D.[4], and Goutal, N.[1]

[1]LHSV, Ecole des Ponts, Cerema, EDF R&D, Chatou, France
[3]Geoscience Ocean Laboratory, University of Western Brittany, IUEM, Plouzané, France
[4]Water Research Laboratory, School of Civil and Environmental Engineering, UNSW Sydney, Sydney, Australia

E-mail addresses: teddy.chataigner@enpc.fr (T. Chataigner), marissa.yates@cerema.fr (M. Yates), nicolas.ledantec@univ-brest.fr (N. Le Dantec), m.harley@unsw.edu.au (M. Harley), k.splinter@unsw.edu.au (K. Splinter), nicole.goutal@edf.fr (N. Goutal)

Keywords: beach morphodynamics, one-line model, longshore transport, shoreline change, sensitivity analysis, wave angle bias

Highlights:
- One-line shoreline change models often produce artifacts in beach planform
- One-line longshore models are highly sensitive to small incident wave angle biases
- Wave angle bias corrections can be obtained using a Monte Carlo approach
- Accurate observations or simulations of wave breaking conditions are necessary

Abstract

The sensitivity of a one-line longshore shoreline change model to the incident wave direction is evaluated at Narrabeen Beach (Australia). As previously observed, the application of the one-line model using wave conditions generated along the 10-m depth contour produces a long-term reorientation of the coastline, with an initial transition period and then a new stable equilibrium during the 10-year period from 2005 to 2015. However, this coastline change in shoreline planform shape is not observed in the shoreline position measurements. The source of this error is investigated by assuming that it is caused by biases in the incident wave direction and by using a Monte Carlo approach to search for the optimal set of wave angle bias corrections to apply at each cross-shore transect. The obtained optimal values enable the one-line model to reproduce accurately the shoreline planform, and they are coherent with estimates of the wave breaking angle obtained independently using a nearshore wave propagation model. Then, using the corrected wave angle time series as a reference, a second Monte Carlo analysis is completed to investigate the sensitivity of the model to errors in the mean wave direction drawn from Gaussian distributions with varying standard deviations. The analysis shows the range of expected errors in shoreline position for an estimated range of errors in the mean wave direction at Narrabeen beach. This work highlights the importance of considering the sensitivity of one-line longshore model simulations to errors in the incident wave angle, which can be relatively large given the uncertainties in spectral wave model estimates of wave direction, in wave buoy observations, and in wave propagation methods or input bathymetry used to estimate wave breaking conditions.

1 Introduction

The littoral zone is a complex environment. It is both a physically dynamic interface, as well as a highly important social and economic zone, given the dense population and high concentration of human activities. In addition, the littoral zone and surrounding coastal areas are highly sensitive to marine flooding and erosion hazards, including shoreline retreat. Thus, it is essential to be able to understand and predict shoreline evolution, in particular at spatial scales of a beach and at medium to long temporal scales, as well as during extreme events.

To achieve this goal, a wide variety of morphological evolution models exist, ranging in complexity from three-dimensional, physics-based models (e.g. MIKE21 (Warren & Bach 1992), Delft3D (Roelvink & Banning 1995), XBeach (Roelvink et al. 2009)) to one-line models representing only cross-shore (e.g. Miller & Dean 2004, Yates et al. 2009, Davidson et al. 2013) or longshore (e.g. Ashton & Murray 2006, Turki et al. 2013, Bouchette et al. 2014) processes. The choice of an appropriate model thus depends on the dominant physical processes that must be represented or parameterized at the spatial and temporal scales of interest, and predicting coastal evolution at seasonal to decadal or longer timescales remains a significant challenge (Safak et al. 2017, Davidson et al. 2017, Montaño et al. 2020). Given the limits of numerical models at these temporal and spatial scales, empirical, process-based models may be an optimal alternative to physics-based models (Murray 2007, Ranasinghe R. 2013, French et al. 2016). This family of models allows simulating shoreline evolution at temporal and spatial scales given their numerical simplicity, low computational cost, and accuracy once calibrated.

At short (e.g. storm) to seasonal timescales, cross-shore processes are often dominant, while over longer time timescales (e.g. interannual to decadal), longshore processes may become increasingly important. To reproduce shoreline changes at these scales, both cross-shore and longshore processes must be taken into account. Recent work has thus focused on developing "hybrid" models that incorporate both cross-shore and longshore processes, including CoSMoS-COAST of Vitousek et al. (2017), LX-Shore of Robinet et al. (2018), the COCOONED model of Antolínez et al. (2019), and the combined model of Tran & Barthélemy (2020). These models are forced by hydrodynamic conditions (e.g. waves) and typically have several free parameters that must be calibrated for each study site.

In hybrid approaches, the one-line longshore transport model is the most commonly used approach to account for longshore processes (e.g., Vitousek et al. 2017, Robinet et al. 2018, Antolínez et al. 2019). For embayed beaches, additional approaches have been developed to simulate longshore processes, including semi-empirical approaches based on decomposing the mean and fluctuating components of the wave field (e.g. Tran & Barthélemy 2020, which is then combined with a cross-shore model), or by modeling directly the beach orientation using an equilibrium approach (Turki et al. 2013, Jaramillo et al. 2021).

Here, the focus is on the classical one-line model, which was first introduced by Pelnard-Considére (1956). It assumes that at long timescales, beach cross-shore profiles maintain an equilibrium shape in balance with the incoming wave field. The beach thus responds to perturbations by restoring the equilibrium shape. Therefore, gradients in longshore sediment fluxes cause landward or seaward shifts in the equilibrium profile, based on the hypothesis that cross-shore processes can be neglected at long temporal scales (Hanson 1989). The longshore sediment flux can be estimated using different formulae (e.g. CERC (1984) (USACE 1984), Kamphuis (1986) (Kamphuis et al. 1986)) that empirically relate the hydrodynamic conditions (e.g. breaking wave height and direction) and the beach geological characteristics (e.g. sediment porosity or grain size) to the longshore sediment flux. This simple approach depends on the quality of both the input data and the choice of model free parameters.

Recently, several studies have focused on identifying and evaluating sources of uncertainties in coastal morphological models. For example, Davidson et al. (2017) tested the sensitivity of the cross-shore empirical model ShoreFor (Davidson et al. 2013, Splinter et al. 2014) to variations in the potential future wave climate. D'Anna et al. (2020) went one step further using the hybrid LX-Shore model (where cross-shore changes are based on the ShoreFor model) by estimating the contribution of different input parameters to the total model uncertainty in a test case applied at Truc Vert beach. In addition, recent studies have also quantified uncertainties related to climate change impacts (Toimil et al. 2020), in particular focusing on the importance of changes in the mean water level on long-term shoreline change (Le Cozannet et al. 2019, Athanasiou et al. 2020).

The one-line longshore model is a simple and therefore widely used model (Larson et al. 1997). It is thus important to study the uncertainties associated with this approach, and several recent studies have investigated the sensitivity of the model to a series of different assumptions and input parameters. Ruggiero et al. (2010) illustrated the relative importance of the wave climate (wave height, peak period and wave direction) and sediment supply (by varying the model sediment flux at the boundary) in simulations with the Unibest model (Delft Hydraulics 1994) by evaluating the model skill in reproducing observed shoreline changes. They showed that altering the offshore mean wave angle generated an important increase in the model error. Kroon et al. (2020) analyzed the relative contribution of errors in different model parameters and wave climate variability to the total model uncertainties as a function of the considered timescales. The model sensitivity to the wave climate is also demonstrated in George et al. (2019), where the longshore flux uncertainties are estimated by incorporating errors in the input wave height and direction. Previous studies have highlighted the sensitivity of the one-line model to wave climate uncertainties, including uncertainties in the wave direction, without directly quantifying the impacts on the modeled shoreline position.

Depending on the inherent complexity of the study site and the quality of the input data, the one-line

longshore model may generate changes in the beach planform (e.g. reorientation) that are different from observations. For example, this was observed recently using hybrid models when modeling shoreline changes in the North Beach Sub-cell of the Columbia River Littoral Cell (Washington, USA, (Antolínez et al. 2019)), and the highly studied Narrabeen Beach (Australia, (Robinet et al. 2020)).

The reorientation "artefact" is corrected for in Antolínez et al. (2019) by replacing the initial shoreline position with the computation of a new long-term average shoreline. This long-term average shoreline is generated by running their hindcast wave climate for 500 years, following Anderson et al. (2018). The authors assume that using the long-term average shoreline as the baseline should correct problems inherited from the wave climate, such as a wave direction bias in the offshore wave conditions or errors in the nearshore wave propagation.

Similarly, in Robinet et al. (2020), the beach reorientation observed in a 5-year-long simulation at Narrabeen Beach is corrected by running the model in two steps. First, the model simulates the 5-year period, and then the final shoreline position at the end of the first simulation is used as the initial shoreline position in the second simulation. The authors assume that the shoreline changes and not the shoreline position simulated in the second step are more accurate. Finally, the simulation results are corrected to account for the difference in the initial shoreline position in order to compare to the observations. Despite applying this two-step method, changes in the shoreline planform shape are still observed in the first year of the second simulation, and this time period is thus excluded from the remainder of their analysis.

These two studies (Antolínez et al. 2019, Robinet et al. 2020) used pre- and post-processing methods to manage the change in the coastline orientation introduced by the one-line longshore model. The authors suggest that the errors are potentially caused by errors in wave direction and/or nearshore propagation. However, they do not attempt to demonstrate this in their work. The current study is focused on understanding the source of the coastline reorientation simulated by the one-line model, as well as applying a simple approach to correct for this error. This work therefore aims to study the overall sensitivity of the one-line modeling approach to biases or errors in the wave conditions. The epistemic uncertainties introduced by the longshore one-line model have two potential sources: the model formulation or the input wave conditions. In this study, it is assumed that the formulation of the one-line model is accurate, and the input wave direction is studied as a potential source of model uncertainties.

Previous studies have used Monte Carlo-based approaches in applications of the one-line model by generating variations in the wave climate based on existing wave distributions (Wang & Reeve 2010, Bergillos et al. 2018) or from measured wave statistics (Reeve et al. 2014, Kroon et al. 2020). Here, two Monte Carlo approaches are used to evaluate the sensitivity of a one-line longshore model to the mean wave direction and wave height at Narrabeen Beach.

~~In the first analysis, a spatially variable, random bias is added to the wave angle time series at each cross-shore transect to find the optimal values minimizing the difference in the simulated and observed shoreline position. Then, the second analysis starts with the wave angle time series corrected with the optimal values obtained in the first analysis, and then adds spatially variable random biases drawn from specified Gaussian distributions to test the sensitivity of the shoreline position results to these types of errors. Here, it is assumed that the distribution of potential errors in measured (e.g. wave buoy observations) or modeled (e.g. large-scale spectral wave models) wave direction are Gaussian. The sensitivity of the one-line longshore model to biases in the wave direction is evaluated by calculating the induced coastline reorientation. This study is applied at Narrabeen beach, where an optimal set of wave angle bias values are estimated to minimize the errors between the observed and modeled shoreline changes. Then, in the second analysis, the impacts of errors in the input wave angle on the modeled shoreline changes are quantified, and although this study is conducted using the data from Narrabeen Beach, the results can be generalized to other sites.~~

In the first analysis, a spatially variable, random bias is added to the wave angle time series at each cross-shore transect to find the optimal values minimizing the difference between the simulated and observed shoreline position. Then, the second analysis aims to test the sensitivity of the shoreline model to spatially variable random biases drawn from specified Gaussian distributions. Here, it is assumed that the distribution of potential errors in measured (e.g. wave buoy observations) or modeled (e.g. large-scale spectral wave models) wave direction are Gaussian. Although this study is conducted using the data from Narrabeen beach, the results can be generalized to other sites.

In the following, the characteristics of the study site are presented (section 2) before describing the one-line longshore model (section 3) and the Monte Carlo approach applied in the analysis (section 4). The optimal bias values and the sensitivity of the model to the input wave angle and wave height are then evaluated (section 5), before discussing the hypotheses and limitations of this study, and the generalization of the approach to other sites (section 6). Finally, a synthesis of the results, as well as perspectives for future studies (section 7) are presented.

2 Study site

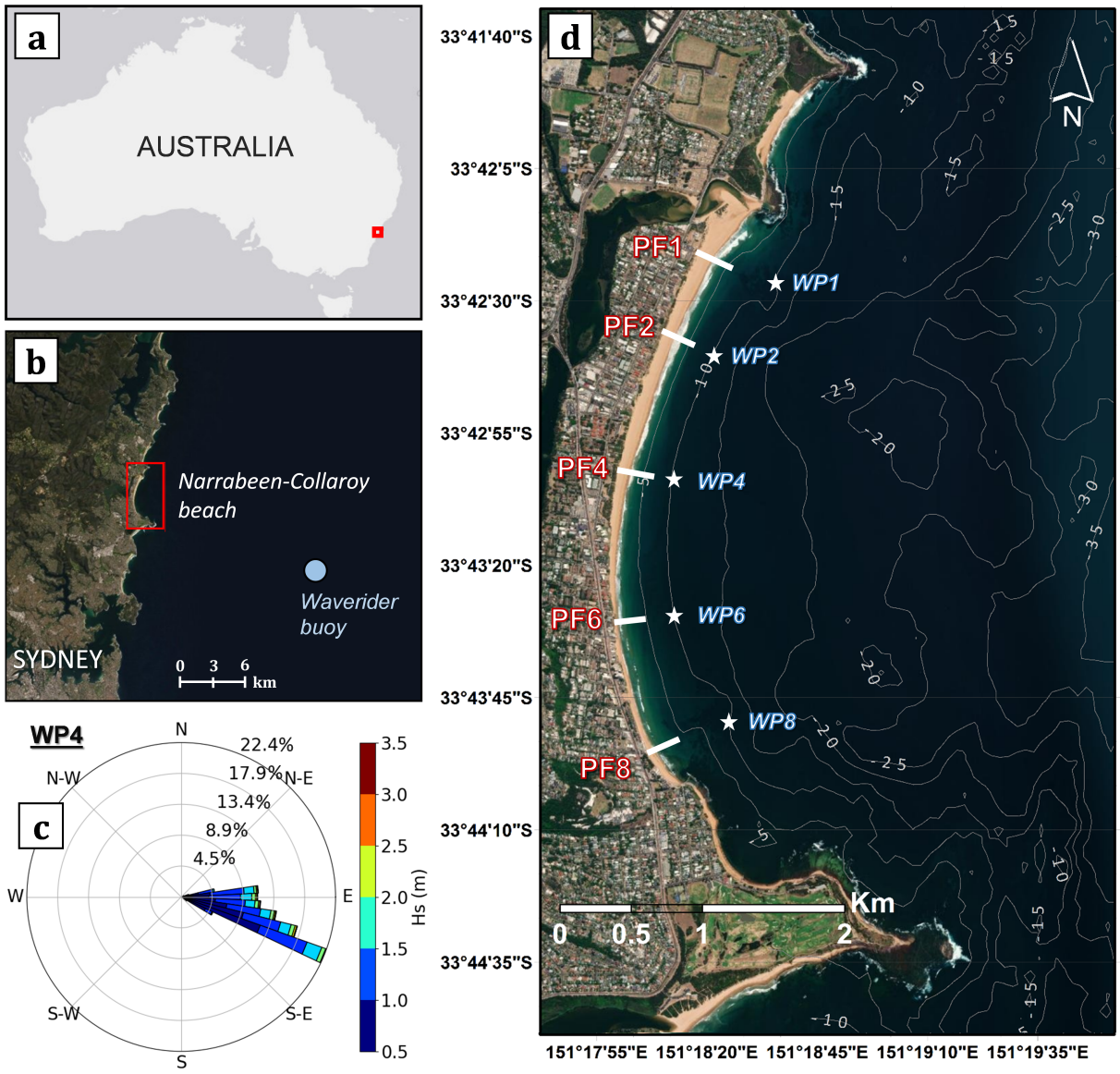

Figure 1: Study site location and wave characteristics: (a) map of Australia indicating the zoom shown in (b), (b) the area around Narrabeen beach, showing the location of Sydney and the offshore wave buoy. (c) The wave rose indicates the percent occurrence of each wave height (colorbar) and wave direction (between 1979-2015), and (d) a satellite image of Narrabeen-Collaroy Beach showing the location of the 5 surveyed cross-shore profiles (named PF1, PF2, PF4, PF6, and PF8) and the 5 locations where wave conditions are available (WP1, WP2, WP4, WP6, and WP8). The bathymetry contours are shown at 5 meter depth intervals (in grey).

The Narrabeen-Collaroy embayment is a 3.6 km-long sandy beach located in southeast Australia, to the north of Sydney (Fig. 1). The embayment consists of Narrabeen beach at the northern end and Collaroy beach at the southern end, and is hereafter referred to as Narrabeen beach for simplicity. The beach is bordered by two rocky headlands at the northern and southern extremities, and the rocky substrate extends underwater to approximately 60 m depth. Reefs are also present from 5 m to 10 m water depth in front of both beach extremities (as can be seen partially in the satellite image in Fig. 1d in front of cross-shore profiles PF1 and PF8). The beach is backed by low dunes at the northern end and by a seawall at the southern end. An estuary forms a lagoon landward of the beach at the northern extremity, and the mouth of the estuary breaches the dune intermittently.

The beach is characterized by fine to medium quartz sand ($D50 \approx 0.3$ mm) that is nearly uniform alongshore (Turner et al. 2016). The headlands at the extremities of the beach and the curvature of the

bay generate alongshore gradients in wave energy caused by wave sheltering and refraction processes. The effects of wave sheltering are more dominant at the southern end of the beach owing to the presence of the 1.5 km-long rocky headland and the predominantly southeasterly incident waves, but wave sheltering also occurs at the northern end of the beach for less-frequent northerly incident waves. Differences in the wave exposure cause differences in the morphodynamic beach state, changing from a higher-energy, longshore-bar trough beach state in the north to a lower energy, low tide terrace/reflective beach state in the south (Wright & Short 1984, Harley et al. 2011).

Narrabeen beach is a semi-diurnal, micro-tidal environment with a mean spring tide of less than 1.5 m. The Sydney waverider buoy, located 11 km offshore in 80 m water depth (Fig. 1b), has recorded directional wave conditions since 1992, which are supplemented by hourly hindcast waves from the Centre for Australian Weather and Climate Research (Durrant et al. 2014) to fill data gaps due to buoy maintenance/dysfunction. The offshore wave climate ranges from moderate to high wave energy (mean H_s $\simeq$1.6 m and T_p $\simeq$10 s), with dominant long-period swell waves impacting the beach from the south-south-east (SSE) direction. In addition, storm waves (defined as $H_s > 3$ m) are generated from tropical cyclones from the northeast, east-coast lows from the east, and cyclones from the south (Turner et al. 2016). The regional wave climate induces a relatively subtle seasonal cycle with higher energy conditions in the austral winter and lower energy conditions in the austral summer. Furthermore, the beach is influenced by the El Niño-Southern Oscillation (ENSO) at interannual timescales (approximately 3 to 7 years), resulting in more energetic and easterly waves impacting Narrabeen beach during La Niña periods and less energetic and more southerly waves during El Niño periods (Harley et al. 2010). Overall, nearshore currents dynamics are primarily driven by waves, given the generally mild wind conditions and microtidal regime.

Beach sand levels have been measured along 5 historical profiles (PF1, PF2, PF4, PF6, and PF8, as shown in Fig. 1d) at approximately monthly intervals since 1976. The offshore wave data is transformed into wave conditions along the 10 m depth contour in front of each profile (Fig. 2c-e) using a look-up table generated with a series of hundreds of SWAN spectral model runs (Turner et al. 2016). This high spatial and temporal resolution dataset consisting of topographic measurements and hourly wave conditions at 5 cross-shore profiles along Narrabeen beach (described in detail by Turner et al. (2016)) is freely available at http://narrabeen.wrl.unsw.edu.au.

Observed morphological changes at the 5 cross-shore profiles show limited long-term changes (maximum linear trend = $-0.54m/yr$ at PF4) in shoreline position (estimated as the cross-shore location of the z=0 m altitude, Harley et al. 2011). However, significant seasonal, annual, and interannual variability is observed, with a mean value of 71 m for the overall range (min/max) of variability of the shoreline position, estimated across all profiles (e.g. PF4 and PF8, Fig. 2a,b). Seasonal variations in shoreline position show primarily accretion during the austral summer and erosion during the austral winter. Offshore of the 10m depth contour, bathymetric variations are nearly negligible, whereas in the surf zone, observed bathymetric variations are on the order of 1m, and thus may influence nearshore wave refraction.

The alongshore differences in wave conditions show more northerly waves and larger wave heights at PF4 than at PF8 (Fig. 2c,e comparing the WP4 and WP8). The peak period (T_p, Fig. 2d) is assumed to be homogeneous along the 10 m depth contour for the 5 alongshore profiles since it is taken as equal to the offshore value (Turner et al. 2016). Fig. 2e also highlights the seasonal dependence of the variability in the wave direction, with reduced variability in wave direction during the austral winter.

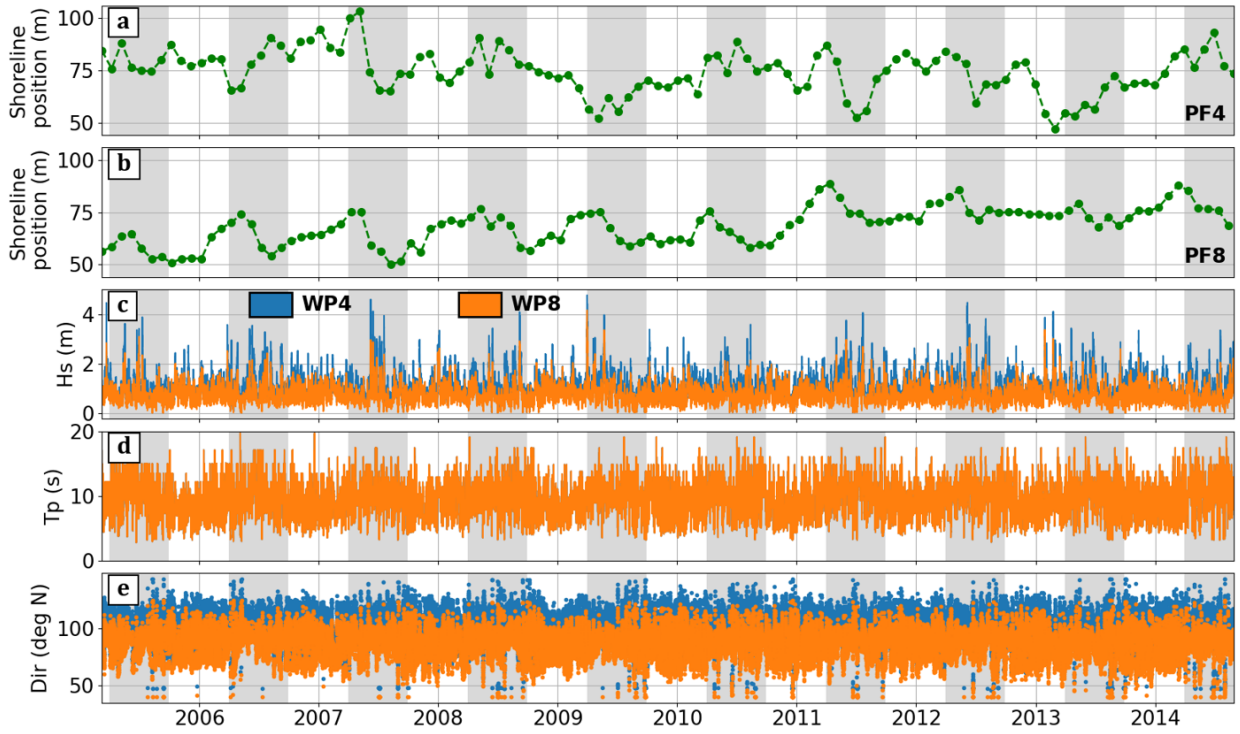

Figure 2: Observations of the shoreline position (z=0 m altitude) at (a) PF4 and (b) PF8, and the corresponding wave conditions at WP4 (blue) and WP8 (orange) showing the: (c) significant wave height (H_s), (d) peak wave period (T_p), and (e) wave direction. The gray-shaded areas indicate austral winters.

3 Model and sensitivity test description

3.1 Mathematical model

In this study, alongshore sediment transport processes are modeled using a simple one-line approach based on the work of Pelnard-Considére (1956). The one-line model estimates changes in the shoreline position S generated by alongshore gradients in the alongshore sediment flux Q:

$$\frac{\partial S}{\partial t} = -\frac{1}{Dc}\frac{\partial Q}{dx}, \tag{1}$$

where Dc is the depth of closure. The longshore sediment flux Q is defined as:

$$Q = Q_0 \sin(2\alpha), \tag{2}$$

where

$$Q_0 = \frac{\rho K H_b^{2.5}\sqrt{g/\gamma_b}}{16(\rho_s - \rho)\lambda}, \tag{3}$$

and

$$\alpha = \alpha_b - \alpha_{shore}. \tag{4}$$

Here, K is a dimensionless empirical parameter, H_b is the breaking wave height, g is the gravitational acceleration, γ_b is the breaker index ratio, ρ and ρ_s are the water and sediment density, respectively, λ is the sediment porosity, and α_b and α_{shore} are the breaking wave angle and the shoreline angle (Fig. 3), respectively. The shoreline angle is calculated as:

$$\alpha_{shore} = \arctan\left(\frac{\partial S}{\partial x}\right). \tag{5}$$

Equation (1) thus can be rewritten as:

$$\frac{\partial S}{\partial t} = -\frac{1}{Dc}\frac{K\sqrt{g/\gamma_b}}{16(\rho_s - \rho)\lambda}\frac{\partial}{\partial x}\left[H_b^{2.5}\sin(2(\alpha_b - \arctan\frac{\partial S}{\partial x}))\right]. \tag{6}$$

The mathematical model is discretized at predefined transects along the coast (Fig. 3), and first-order, centered finite difference schemes are used:

$$\frac{S_n^{i+1} + S_n^i}{\Delta t} = -\frac{1}{Dc}\frac{Q_{n+1/2} - Q_{n-1/2}}{\Delta X_n}. \tag{7}$$

As shown in Fig. 3, n is the transect index, X_n is the alongshore distance between adjacent transects, and i is the time index.

~~Following Robinet et al. (2018), the wave characteristics at breaking (e.g. H_b, α_b, and γ_b) are calculated by numerically refracting and transforming the wave conditions from 10m water depth (e.g. WP points shown in Fig. 1d) using the method of Larson et al. (2010).~~

The wave characteristics at breaking (e.g. H_b, α_b, and γ_b) are calculated by numerically refracting and transforming the wave conditions from 10 m water depth (e.g. WP points shown in Fig. 1d) using the method of Larson et al. (2010). The limitations and hypotheses of this empirical approach are discussed in Section 6.

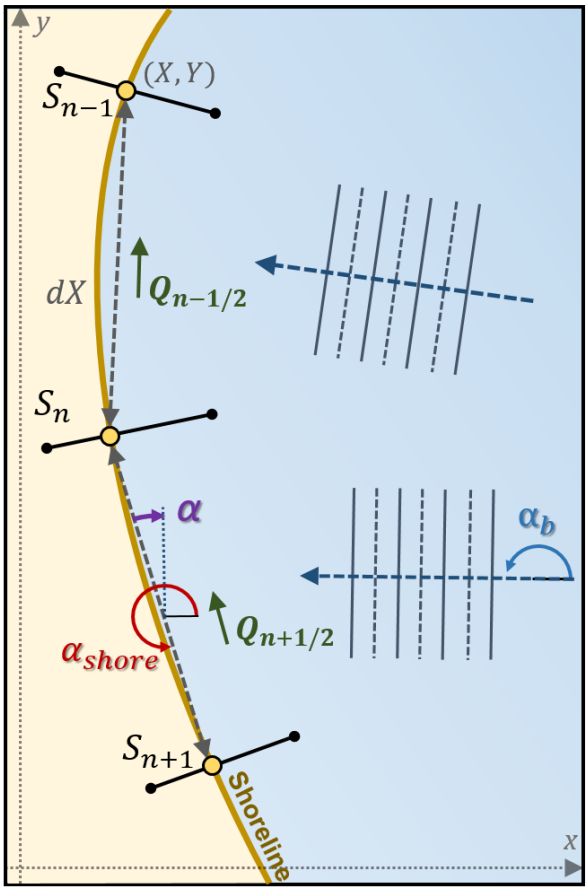

Figure 3: Schematic representation of the model setup for cross-shore transects (index n), showing the shoreline position S, the relative wave angle α (Eq.4), the alongshore sediment flux Q, and the local reference frame (X, Y).

3.2 Model application at Narrabeen Beach

The one-line longshore model is applied at Narrabeen beach at 15 cross-shore transects distributed uniformly alongshore ($\Delta X = 250$ m). Wave conditions along the 10m depth contour were interpolated from the time series provided at the 5 cross-shore profiles. Wave time series are unavailable at the 2 boundary transects, so the wave conditions at these locations are initially assumed to be the same as those of the adjacent profiles.

Although measurements of sediment fluxes at the domain boundaries are unavailable, given the presence of the rocky outcrops limiting alongshore sediment transport, they are assumed to be small, and zero-flux conditions are applied at the boundaries. This hypothesis will be discussed further in section 6.

The K parameter is set to 0.02 for all transects based on qualitative comparisons of the amplitude of simulated and observed shoreline position variability. This parameter is often difficult to determine, and typical values in the literature range between 0.014 and 2.3 (Pilkey & Cooper 2002). The relative contribution of the K parameter in this study will be discussed further in section 6. The depth of closure Dc is estimated using the formula proposed by Hallermeier (1983), and an alongshore mean value of 12 m is used for all transects in agreement with the bathymetric observations of Turner et al. (2016).

The one-line model is applied for a 10-year time period, from 2005 to 2015, to simulate shoreline changes caused by longshore processes using a hourly time step. Cross-shore processes are neglected by assuming that they are dominant at interannual timescales and do not contribute significantly to observed trends at pluriannual timescales. Harley et al. (2015) completed an EOF (empirical orthogonal function) analysis of 5 years of extensive 2D topographic surveys, identifying two principal modes of shoreline variability: cross-shore migration and beach rotation, explaining 55% and 22% of the variance, respectively. Beach rotation is typically attributed to longshore sediment processes, but the authors suggested that alongshore variability in cross-shore processes and differences in sandbar dynamics may also contribute. However, the contributions of these processes are not able to be quantified, and the temporal mode of the beach rotation EOF shows seasonal oscillations and no significant long-term trends.

Thus to compare the observations and the model, the mean annual shoreline position $\bar{S}(t)$, where the overline indicates the mean over a 12-month period, is calculated to focus predominantly on longshore processes and to evaluate the long-term trends in shoreline position. The simulation shows that, when forced with the wave time series along the 10 m depth contour, the one-line model causes a change in the shoreline planform shape, as seen in (Fig. 4b), where the final annual mean simulated ($\bar{S}_{f,mod}$) and observed ($\bar{S}_{f,obs}$) shoreline position are compared.

In comparison to the observed shoreline position at the end of the simulated time period, the simulated coastline shows significant erosion at the southern end (around 150m at PF8), nearly no difference in the middle of the beach (with a pivot point near PF6), and accretion at the northern end (between +30m to +60m between PF1 and PF4)(Fig. 4b). Similar results producing large changes in the beach planform shape were also observed by Robinet et al. (2020) (as discussed previously) with the LX-Shore hybrid model over the 5-year time period from 2005 to 2010.

The beach reorientation simulated by the one-line model is caused by a disequilibrium between the coastline orientation and the incident wave direction. For a simplified case with a constant wave incidence angle, the one-line model is equivalent to a diffusion equation, bringing the shoreline position toward an equilibrium state. This equilibrium is reached when the coastline orientation is perpendicular to the incident wave direction. When the one-line model is applied at a natural site with temporal variations in the wave direction, the same response is achieved if the mean incident wave direction does not vary significantly in time. Thus, assuming that the one-line model concept is correct, the simulated beach reorientation observed here is hypothesized to be caused by errors in the model input variables or parameters, and in particular by biases in the incident wave direction. The potential contribution of bias errors in the wave height will be also be discussed in section 6.

4 Methods: wave angle bias assessment

To evaluate the sensitivity of the model to the incident wave angle, two different analyses are completed by: (1) first searching for the optimal set of bias values that minimize the differences between the simulated and observed shoreline evolution, and then (2) systematically testing the sensitivity of the model to sets of random wave angle biases generated from specified Gaussian distributions. For both analyses, Monte Carlo simulations are completed to evaluate the impacts of the wave angle biases on the simulated shoreline position and resultant coastline orientation.

In this analysis, it is important to distinguish between a wave angle bias and a wave angle error. A wave angle bias is variable in space but constant in time (systematic error), whereas a wave angle error is variable in both space and time (non-systematic or random error). In this study, wave angle biases are examined because in the long term, random wave angle errors were observed to compensate for each other in time (not show here) and did not generate long-term coastline reorientation in the one-line longshore model, as will be discussed further in section 6.4.

4.1 Wave angle bias estimation

In the first analysis, the impact of wave angle biases in the input wave time series at 10 m depth is evaluated with a 3-step method.

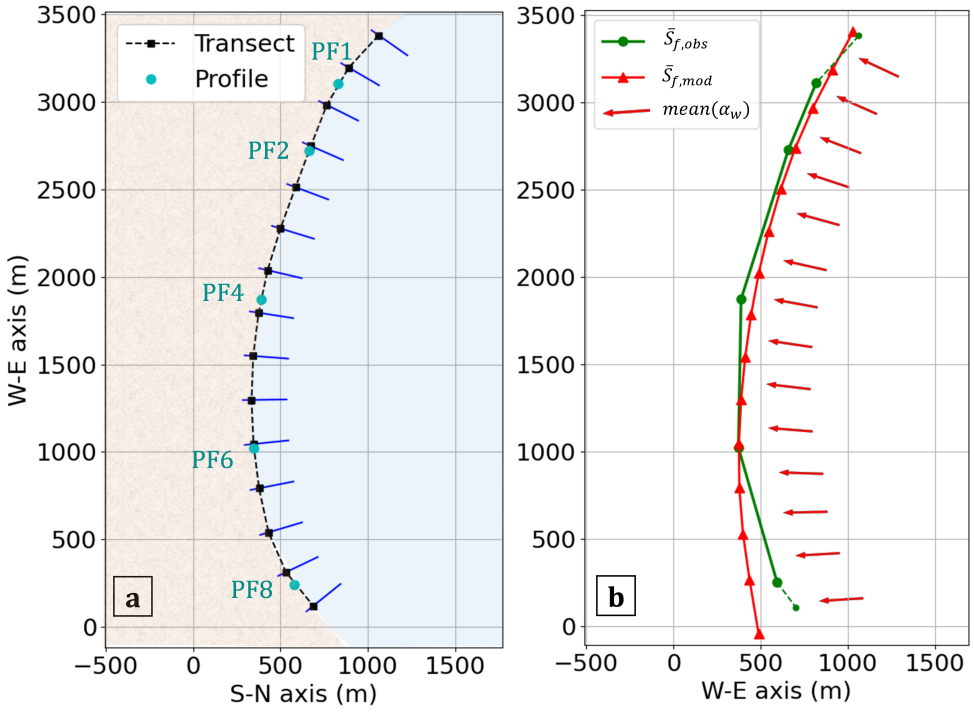

Figure 4: (a) Longshore model setup at Narrabeen beach, showing the 15 defined cross-shore transects. (b) Observed (green line) and simulated (red line) annual mean shoreline position at the end of the 10-year simulation. For each cross-shore transect, the red arrow indicates the temporal mean wave angle (α_w) at 10 m water depth.

First, at each position between adjacent transect, a random wave angle bias (τ) that is constant in time, is drawn from a uniform, univariate distribution using a Monte Carlo approach. The uncorrelated random wave angle biases ($\tau_{n+1/2}$) are then added to the wave direction time-series at each position $n + 1/2$ such that the new wave angle $\tilde{\alpha}_{w,n+1/2}(t)$ in 10 m water depth is:

$$\tilde{\alpha}_{w,n+1/2}(t) = \alpha_{w,n+1/2}(t) + \tau_{n+1/2}. \tag{8}$$

Then, the one-line longshore model is run using the modified wave direction time series $\tilde{\alpha}_{w,n+1/2}(t)$, while the input wave height $H_{s,10}$ and wave period $T_{p,10}$) remain unchanged.

Lastly, the normalized root mean square error (NRMSE) is computed to quantify the difference between the observed and simulated shoreline position. The root mean square error (RMSE) is computed as:

$$RMSE = \sqrt{\sum_{n=1}^{N}\sum_{t=1}^{T}\left(\bar{S}_{mod,n}(t) - \bar{S}_{obs,n}(t)\right)^2} \tag{9}$$

with $\bar{S}_{obs}$ the annual moving average observation (to remove the seasonal variability) computed every month and $\bar{S}_{mod}$ the simulated shoreline position at the corresponding time, summed over all observations times T and all transects N.

The NRMSE is calculated as the RMSE normalized by the minimum of the all the RMSE values after the Monte Carlo process. This method is applied twice, in a nested approach. A first set of 15,000 Monte Carlo realizations of wave angle biases is generated, allowing τ to vary from -30° to +30°, following a uniform univariate distribution. The results are then used to define smaller angle intervals for each transect $n + 1/2$ (as shown by the vertical cyan bars in Fig. 5a), and a second set of 10,000 Monte Carlo realizations were completed to determine the set of wave angle biases $\tau_{n+1/2}$ yielding the minimum NRMSE.

Since morphological observations are not available at the domain boundaries during the simulated period, the existing 2D survey data, which spans part of the simulated period, are used to estimate the long-term trends at the two boundary transects. No trends are observed, thus it is assumed shoreline position remains unchanged for the 10-year period.

4.2 Model sensitivity analyses

In order to test the sensitivity of the model to the magnitude of the wave angle bias, the wave angle time series $\tilde{\alpha}_{w,n+1/2}(t)$ are corrected using the optimal set of biases obtained in the previous analysis. These new time series are then used as the reference simulation in the sensitivity analyses. Then, new randomly generated wave angle biases $\tau'_{n+1/2}$ are drawn from Gaussian distributions with specified standard deviations and are added to each cross-shore transect. The new wave angle time series $\alpha'_{w,n+1/2}(t)$ at each cross-shore transect are thus defined as:

$$\alpha'_{w,n+1/2}(t) = \tilde{\alpha}_{w,n+1/2}(t) + \tau'_{n+1/2}. \tag{10}$$

For each test, the $\tau'_{n+1/2}$ values are drawn from independent Gaussian distributions with a specified standard deviation $\sigma_{\tau'}$. Six different tests with 1000 Monte Carlo realizations were carried out for $\sigma_{\tau'}$ ranging from 1° to 6°.

A second sensitivity analysis testing the relative importance of biases in the wave height is carried out for comparison. The same approach is used, and the wave height time series are adjusted by a bias β' that is a percentage of the wave height, such that:

$$H'_{sw,n+1/2}(t) = (1 + \beta'_{n+1/2})H_{sw,n+1/2}(t). \tag{11}$$

For each test, the $\beta'_{n+1/2}$ values are drawn from independent Gaussian distributions with a specified standard deviation $\sigma_{\beta'}$. Four different tests with 1000 Monte Carlo realizations were carried out for $\sigma_{\beta'}$ ranging from 5% to 30%.

Finally, the associated error is quantified as the difference between the final, simulated annual mean shoreline position for each realization with a specified $\sigma_{\tau'}$ or $\sigma_{\beta'}$ and for the reference simulation.

The distribution of the differences is obtained for each value of $\sigma_{\tau'}$ or $\sigma_{\beta'}$, which is then characterized by its standard deviation $\sigma_{\Delta S}$. The standard deviation serves as a metric to estimate the order of magnitude of shoreline position errors for a given distribution of wave angle bias errors.

5 Results

5.1 Optimal wave angle analysis

In Fig. 5a, the 50 best Monte Carlo realizations with a NRMSE within 30% of the minimum value vary within a range of up to 10° for each transect and show generally positive values of τ in the north (with two exceptions just north of PF2 and PF4), and then increasingly negative values south of PF4. The optimum set of τ values (purple curve, Fig. 5a) between PF1 to PF8 ranges from 10° to -20° (Table 1).

Table 1: Approximate optimum set of τ values for each cross-shore profile that minimize the NRMSE between the simulated and observed shoreline changes.

Profile	PF1	PF2	PF4	PF6	PF8
Optimum τ	-0.5°	4.8°	4.5°	-13.2°	-19.9°

It is important to note that the model depends not only on $\tau_{n+1/2}$, but also on alongshore gradients in $\tau_{n+1/2}$. In the one-line longshore model, changes in the shoreline position are caused by alongshore gradients in the sediment flux, which are calculated from alongshore gradients in the wave angle α_b and in the wave height H_b, as shown in Eq.(7). The alongshore gradients in $\tau_{n+1/2}$ for the 50 best realizations (Fig. 5b) have a similar, concave shape with the highest values at the extremities of the beach.

The optimal τ values correct for the potential wave angle bias at breaking, caused either by biases in the 10 m depth wave time series or by wave refraction occurring between the 10 m depth contour and the wave breaking point. The large values of $\tau_{n+1/2}$ obtained near the boundary transects (Fig. 5a) may also be attributed to two additional sources that impact more significantly the transects at or near the domain boundaries. They correct for errors induced by extrapolating the wave conditions from the WP points to the domain boundaries, likely generating the largest errors at these transects. They also correct for the assumption that there are no sediment fluxes at the boundaries.

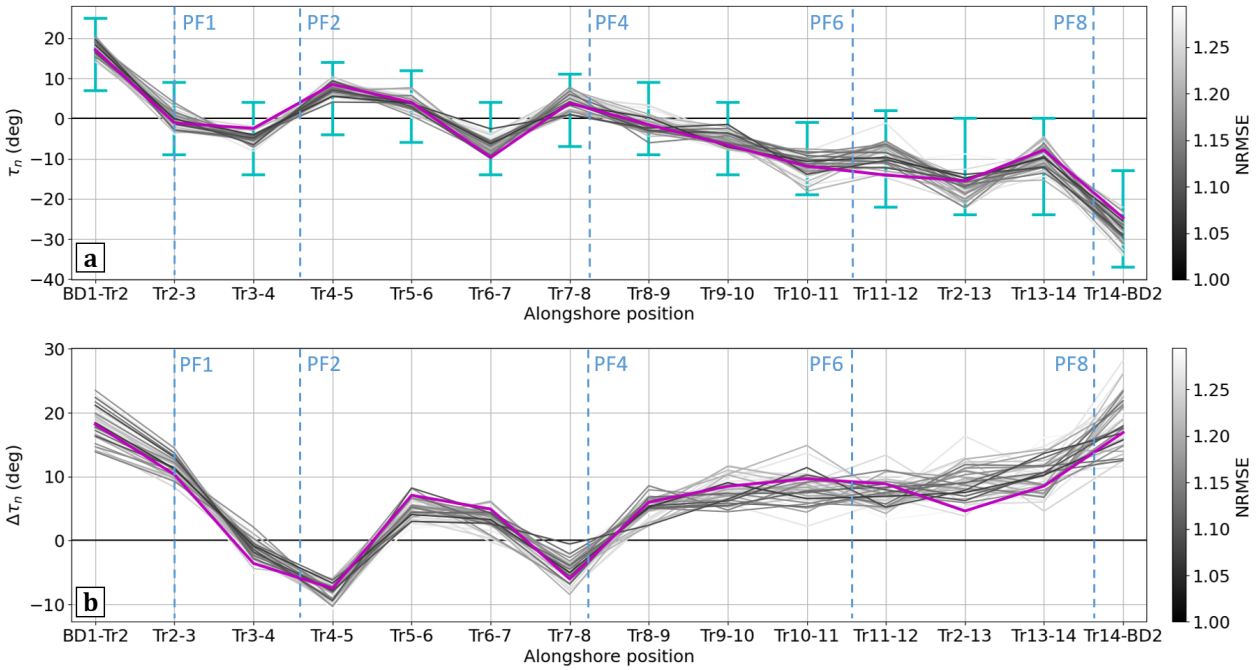

Figure 5: Wave angle bias tests: (a) wave angle bias correction ($\tau_{n+1/2}$) and (b) gradient in wave angle bias correction between adjacent transects plotted for the 50 best Monte Carlo realizations. The vertical cyan bars indicate the range of values used to define the second set of refined Monte Carlo realizations. The color of each curve indicates the NRMSE (gray color scale ranging from 1.0 to 1.3), and the optimal set of $\tau_{n+1/2}$ values are shown in magenta.

5.2 Optimal wave angle bias values

Using the optimal set of $\tau_{n+1/2}$ values in the one-line longshore model reproduces a simulated coastline shape similar to the observed coastline shape (Fig. 6a). The wave angle time series are corrected with small changes in the mean wave angle (e.g. Table 1 for PF1-PF8) relative to the original mean wave angle (Fig. 6a), except close to the domain boundaries at the extremities of the beach. The difference between the annual mean initial, observed and final, observed or modeled shoreline position is calculated as: $\Delta\bar{S} = \bar{S}_f - \bar{S}_i$. The difference $\Delta\tilde{\bar{S}}$ calculated for the corrected wave time series is similar to the observed changes $\Delta\bar{S}_{obs}$ (Fig. 6b).

The simulated shoreline position changes using the original wave angle time series ($\alpha_{n+1/2}$ red triangles in Fig. 6b) are generally larger than or of the same order of magnitude as the seasonal variability over the 10-year period (Fig. 6b, gray bars). However, the simulated shoreline position changes using the corrected wave time series are smaller than the observed seasonal variability (Fig. 6b, gray bars) and agree more closely with the observations. Finally, this simple analysis demonstrates how a relatively small bias in the input wave angle can cause significant changes in the shoreline planform shape that are different from the observations.

5.3 Model sensitivity analyses

Using the wave angle time series $\tilde{\alpha}_w$ corrected with the optimal set of bias values $\tau_{n+1/2}$ as the reference case, a sensitivity analysis is completed to evaluate the impacts of randomly distributed wave angle biases on the simulated shoreline position.

Six different tests of 1000 Monte Carlo realizations were carried out for $\sigma_{\tau'}$ ranging from 1° to 6°, and the model error is quantified as the standard deviation $\sigma_{\Delta S}$ of a Gaussian distribution fit to the distribution of the estimated shoreline position differences (e.g. Fig. 7a,c, for $\sigma_{\tau'} = 5°$). The standard deviation of shoreline position errors $\sigma_{\Delta S}$ increases approximately linearly as a function of the standard deviation of the wave angle biases $\sigma_{\tau'}$ (Fig. 7b).Shoreline position errors are on the order of 5m for wave angle biases as small as 1°, and increase to more than 30m for wave angle biases of only 5-6°.

With respect to the sensitivity of the model to a bias in the wave height, with $\sigma_{\beta'} = 5\%$, 10%, 20%, 30%, the associated shoreline position errors $\sigma_{\Delta S}$ are approximately one order of magnitude smaller than for the wave angle bias tests (comparing Fig. 7d, e and f). For example, shoreline position errors are typically less than 1m for wave height biases of 5% and reach only 3m for wave height biases as large as 30%.

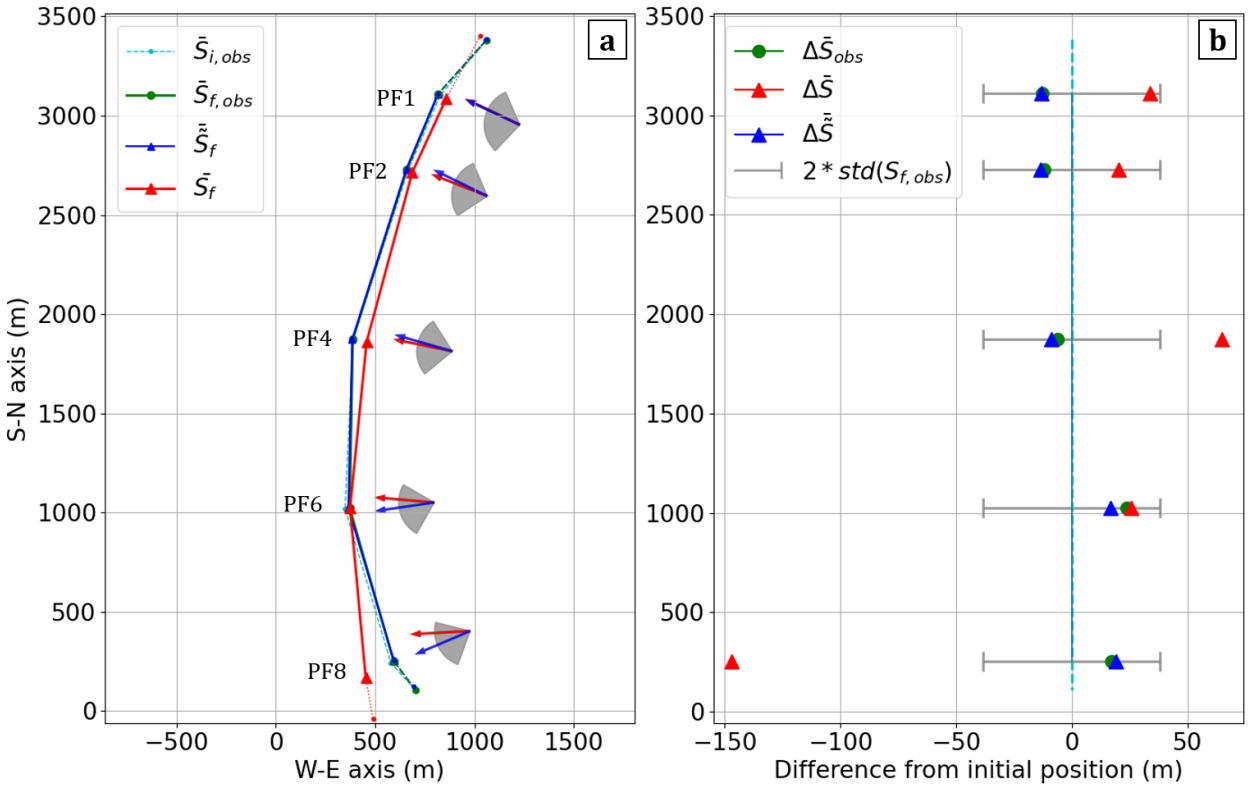

Figure 6: Comparison of the observed and simulated shoreline position: (a) aerial view of the observed initial $\bar{S}_{i,obs}$ (cyan) and final $\bar{S}_{f,obs}$ (green) shoreline position and the simulated final shoreline position for the original $\bar{S}_f$ (red) and corrected $\tilde{\bar{S}}_f$ (blue) wave angle time series. Also shown are the temporal mean wave direction of the original α_w (red arrow) and corrected $\tilde{\alpha}_w$ (blue arrow) time series and the wave direction envelop (grey shading) in 10 m water depth. (b) Difference in the shoreline position relative to the initial observations (cyan) for: the final observed ($\Delta\bar{S}_{obs}$, green) and simulated shoreline position for the original ($\Delta\bar{S}$, red) and corrected ($\Delta\tilde{\bar{S}}$, blue) wave angle time series, and beach shoreline position variance (gray).

6 Discussion

6.1 One-line model limitations

The one-line longshore model is a simple approach for estimating large-scale longshore sediment transport that has several important conceptual limitations (see Pilkey & Cooper 2002). Two potential sources of error can be distinguished: the conceptual framework of the one-line model and the longshore flux estimation.

In the conceptual model, one limitation is the estimation of the depth of closure Dc, which determines the active profile length. The assumption that a well-defined depth of closure exists remains controversial, and it is difficult to identify this limit *in situ*. While a physical, cross-shore limit to the active profile (zone within which wave-breaking induced sediment transport occurs) likely exists, this limit varies in time as a function of the wave characteristics and sediment characteristics and availability, and depends on the considered time period (Valiente et al. 2019). Therefore, assuming a constant value in time and in space (e.g. for a beach) is convenient for modeling purposes but may contribute to intrinsic errors in one-line models (D'Anna et al. 2021). A second limitation is the assumption of a constant equilibrium profile and a uniform cross-shore distribution of the longshore sediment flux (Bayram et al. 2001). In addition, factors like the instantaneous tide level, which would be more important on a meso- or macrotidal beach, or total water depth likely impact the cross-shore distribution of sediments.

In estimating the longshore sediment flux, a second potential source of errors in the one-line model is the choice or calibration of the K parameter in the CERC formula. This free parameter determines the longshore flux magnitude, and its magnitude and even use are highly controversial (see Pilkey & Cooper 2002). However, in this study the value of K does not impact the estimation of τ since K is constant for all transects and thus the one-line model can be simplified to a diffusion equation. Therefore, in long-term simulations where the coastline reaches a new equilibrium shape, the K value primarily impacts the value of

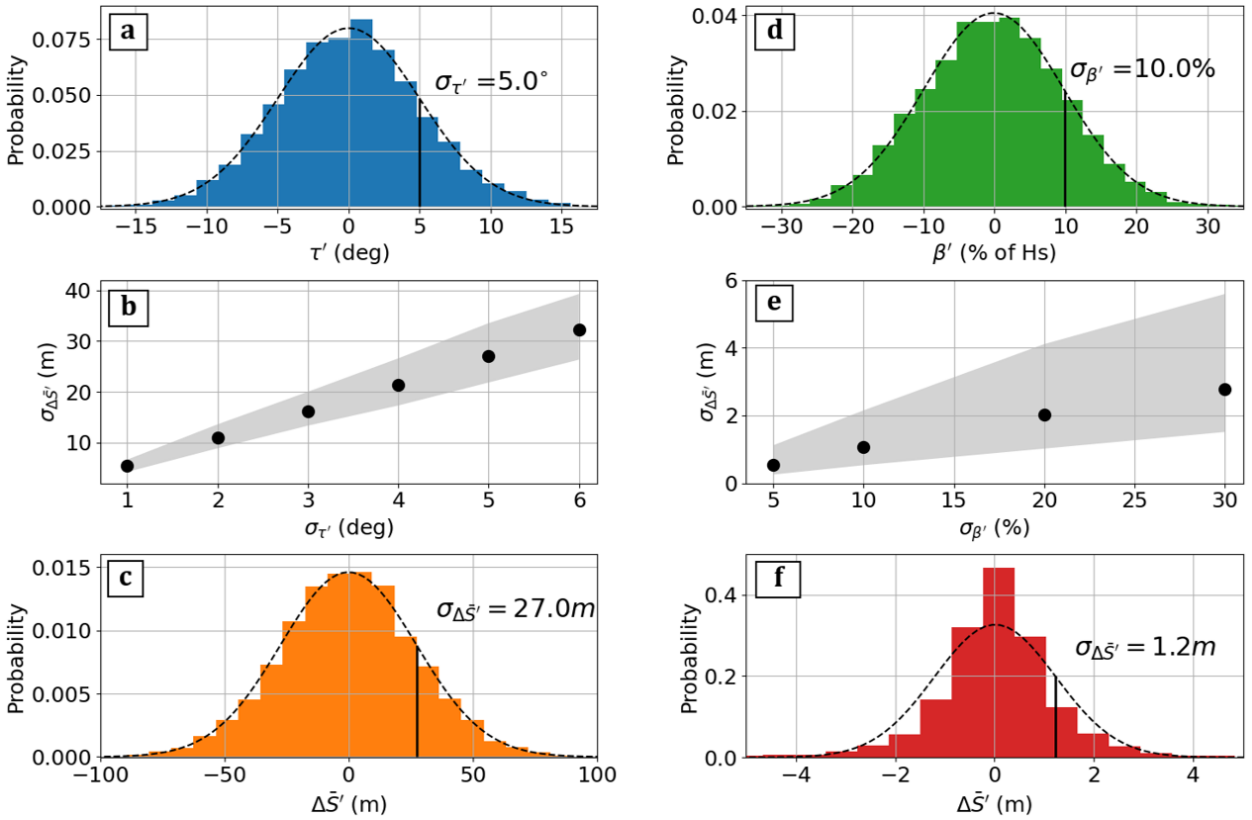

Figure 7: Wave angle bias sensitivity analysis: (a) wave angle bias distribution for $\sigma_{\tau'} = 5°$, (b) standard deviation of shoreline position differences ($\sigma_{\Delta\bar{S}'}$) as a function of $\sigma_{\tau'}$, showing the mean (black stars) and envelope (range of minimum and maximum values) over all transects (gray shading) (c) shoreline position difference (in comparison to the reference case) distribution for all transects for $\sigma_{\tau'} = 5°$, (d) β' distribution for $\sigma_{\beta'} = 10\%$, (e) standard deviation of shoreline position differences ($\sigma_{\Delta\bar{S}'}$) as a function of $\sigma_{\beta'}$, showing the mean (black stars) and envelope (range of minimum and maximum values) over all transects (gray shading), and (f) shoreline position difference distribution for all transects for $\sigma_{\beta'} = 10\%$.

the diffusion coefficient, which controls the coastline adjustment timescale to changes in the wave direction, but does not impact the coastline shape.

Finally, the one-line model conserves sediment, and therefore the choice of boundary conditions may have strong impacts on the simulated shoreline changes. In this study, it is assumed that there are no sediment fluxes at the boundaries since the beach is bounded by rocky outcrops. The only likely sediment sources or sinks are associated with the lagoon mouth at the northern end of the beach. However, the corresponding fluxes are unable to be quantified accurately and are assumed to be negligible in comparison to the estimated longshore fluxes (Harley et al. 2011), so they are not considered in the model.

6.2 Wave bias analysis assumptions and limits

In this study, several assumptions are made in applying a Monte Carlo approach to finding the optimal set of wave angle bias corrections and then in completing sensitivity analyses to randomly generated wave angle and wave height bias errors. Firstly, it is assumed that the errors observed in the one-line model simulation (e.g. reorientation of the coastline) are caused by errors in the input wave angle time series and not in the general model formulation.

This study focused on evaluating the effects of random wave angle biases rather than random, time-variable errors because in preliminary tests (not shown here), the effects of random wave angle errors compensated for each other in time over the 10-year period, causing no long-term trends in shoreline position changes. Time-variable errors induce short-term shoreline changes, at timescales of the model time-step, which are affected by the K parameter. Thus, the sensitivity of the model to time-variable errors is linked intrinsically to the estimation of K, and therefore these two issues should be addressed simultaneously (as in Kroon et al. 2020).

Secondly, a Monte Carlo approach is chosen to generate the random wave angle biases $\tau_{n+1/2}$. A simpler

hypothesis would be to consider an alongshore homogeneous τ, assuming that the wave angle bias originates at the wave buoy and remains constant as the waves propagate to the 10m depth contour. In this case, the corrected wave angle time series would become:

$$\alpha *_{w,n+1/2}(t) = \alpha_{w,n+1/2}(t) + \tau. \tag{12}$$

The effects of adding an alongshore homogeneous τ (ranging from $-30° \leq \tau \leq 30°$) show that it is insufficient to correct changes in the shoreline planform shape because it induces different responses at different alongshore locations. For example, an alongshore homogeneous change in mean wave direction is able to correct the shoreline position changes at PF8 with $\tau \approx -10°$ (Fig. 8b), but it is unable to do so at PF4 (Fig. 8a). At PF4, adding a spatially homogeneous τ value does not allow reproducing the observed shoreline changes since all of the simulations predicted significant long-term trends that were not observed.

At Narrabeen beach, local wave refraction contributes to alongshore gradients in wave angle. Alongshore variable biases thus allow to correct for errors associated with local wave refraction that varies alongshore owing to the curvature of the coastline and the alongshore variable bathymetry. In particular, these errors may become large at the extremities of the beach near PF1 and PF8 where reefs located in -5 to -10 m water depth likely have significant impacts on wave refraction.

Extending this work beyond Narrabeen beach, this analysis emphasizes the importance in representing well not only the wave angle time series, but also alongshore gradients in the wave angle time series used to force one-line longshore models.

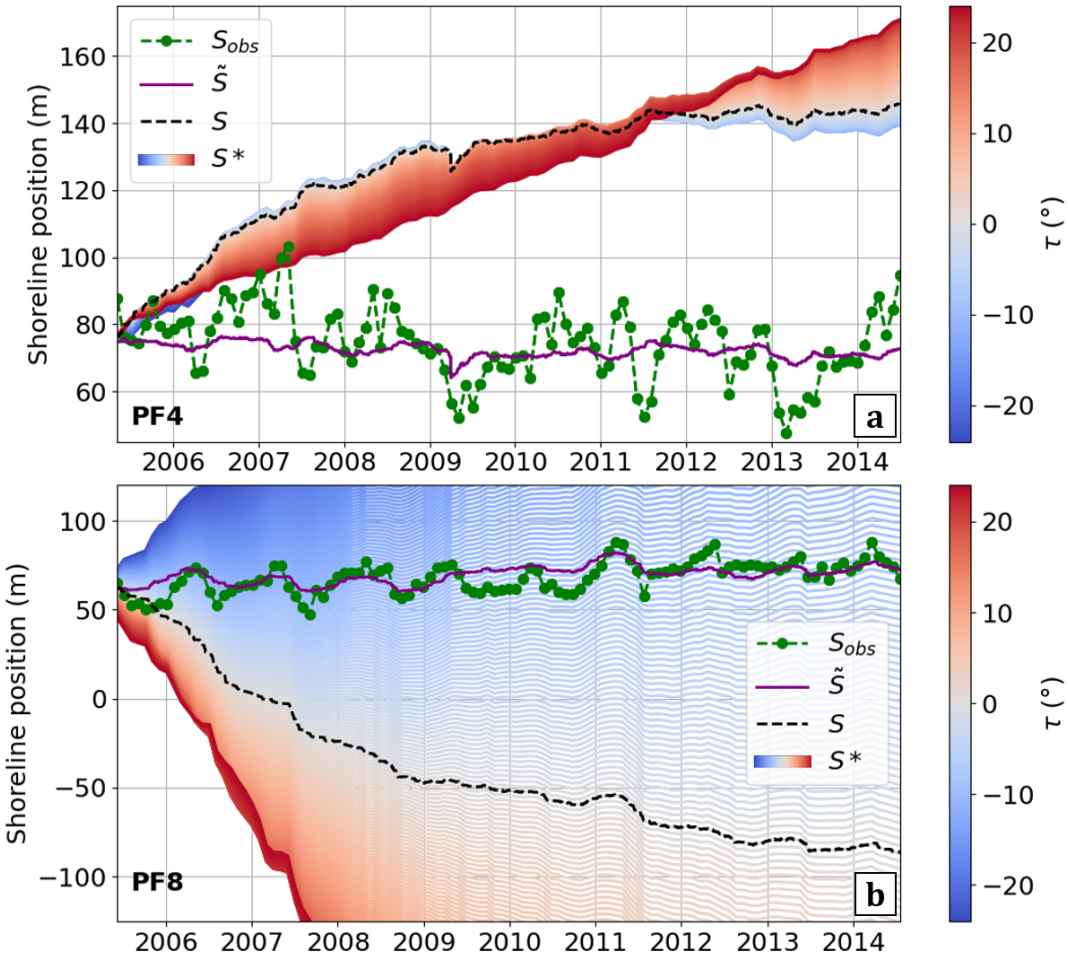

Figure 8: Sensitivity analysis with alongshore homogeneous τ showing the shoreline position evolution from observations S_{obs} (green), the original model simulation S (black), the model simulation forced with the corrected wave angle time series $\tilde{S}$ (purple), and the model simulations S^* forced with wave angle time series adjusted with alongshore homogeneous τ ranging from $-30°$ to $30°$ (blue-red colorbar).

6.3 Planform beach orientation

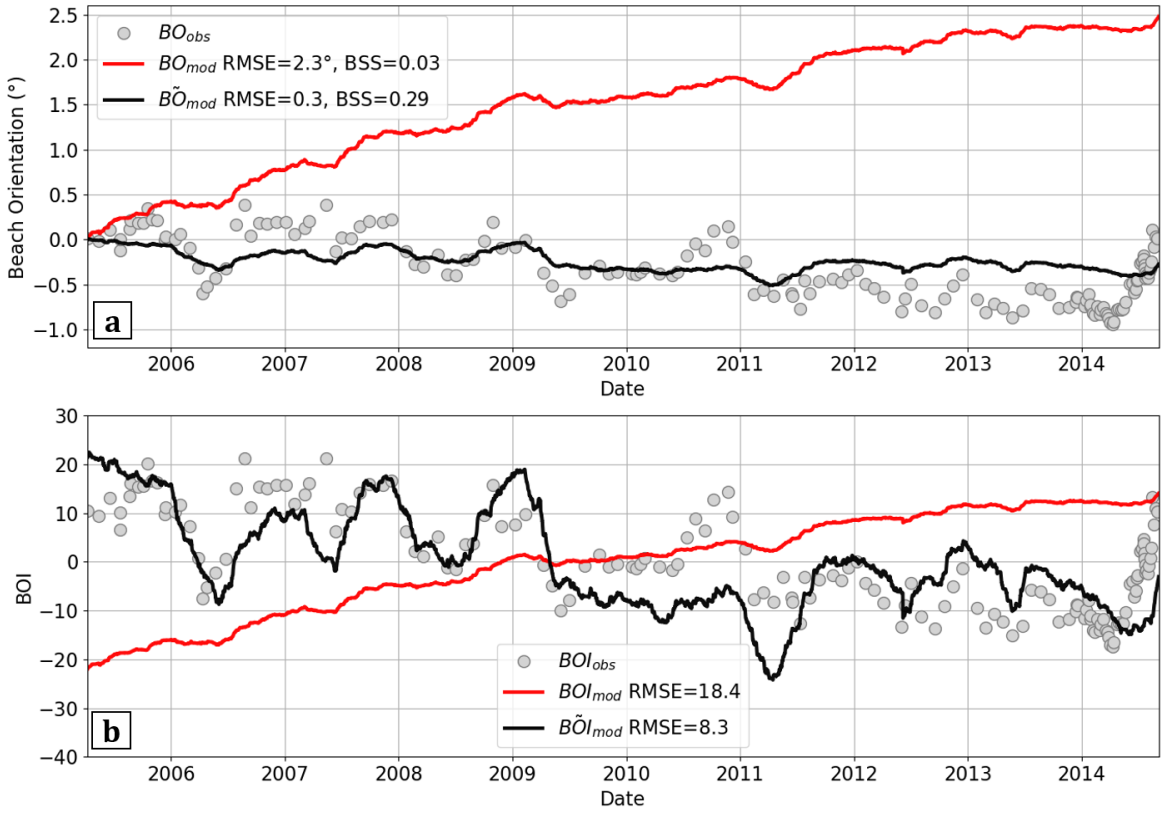

Figure 9: Comparison of (a) Beach Orientation (BO) and (b) Beach Orientation Index (BOI) for shoreline observation (grey dotted), original model simulation (red) and model simulation forced with correct wave angle time series (black).

To evaluate the capacity of the one-line model to accurately reproduce the beach orientation and it evolution in time, the Beach Orientation BO and Beach Orientation Index BOI were calculated following Harley et al. (2014) and Jaramillo et al. (2021). The BO and BOI are calculated using the observed shoreline position S_{obs} and both the original S and corrected $\tilde{S}$ simulated shoreline positions at the 5 cross-shore transects PF1-8 (Fig. 9a, b). During the simulated period, the observed beach orientation BO_{obs} and beach orientation index BOI_{obs} show slightly negative trends and small seasonal oscillations (gray circles, Fig. 9). In comparison, beach orientation BO_{mod} and beach orientation index BOI_{mod} calculated from the simulations with the original wave angle time series (red curves, Fig. 9) shows significant differences with the observations. After correcting the wave angle time series with the optimal set of biases, the agreement between the observed and simulated beach orientation $\tilde{BO}_{mod}$ and beach orientation index $\tilde{BOI}_{mod}$ (black curves, Fig. 9) increases significantly. Jaramillo et al. (2021) also modeled shoreline changes at Narrabeen beach with an equilibrium-based shoreline rotation model, quantifying their model performance with the $RMSE$ between the simulated and observed BO and BOI time series. The results presented here (using only a one-line longshore model) obtain $RMSE$ of the same order of magnitude as their study (which covered a longer time period).

6.4 One-line model sensitivity to biases in the wave height and direction

Assuming that the one-line model is conceptually correct, this work shows that correcting a small wave angle bias (approximately 5-10°) has significant impacts on simulated long-term shoreline change trends. The comparison of the observed and corrected simulations of shoreline changes highlights that this approach allows improving long-term (10-year) simulations of shoreline evolution ($\tilde{S}$, purple line compared to S_{obs}, the dashed black line in Fig. 8). As expected, the corrected mean wave angles in Fig. 6a are more perpendicular to the coastline orientation. However, the difference between the mean wave and shoreline angles is not reduced to zero, which would result in no longshore sediment fluxes.

The sensitivity analyses quantified the impacts of a Gaussian distribution of wave angle biases in wave direction and wave height. The wave angle sensitivity analysis showed significantly larger impacts on the modeled final shoreline position than the wave height sensitivity analysis. For wave angle biases τ' drawn from a Gaussian distribution with a standard deviation of $\sigma_{\tau'}$, the associated alongshore gradients in wave direction are even larger, following a Gaussian distribution with a standard deviation of $\sqrt{2}\sigma_{\tau'}$. The observed increases in $\sigma_{\Delta\bar{S}'}$ are thus a result of the importance of alongshore gradients in wave angle and wave height in the one-line model, as well as the uncorrelated sampling method used to obtain each Monte Carlo realization. These gradients thus cause large gradients in alongshore sediment fluxes, resulting in significant shoreline position changes (e.g. on the order of 5 m to 30 m for wave angle biases ranging from 1° to 6°).

In this study, the set of optimal τ values (section 5.1) are the same order of magnitude as the uncertainties estimated by Turner et al. (2016) for transects PF1, 2, 4, and 6. The higher τ values obtained at PF8 and near the boundary transects BD1 and BD2 are likely caused by other factors, as suggested in section 5.1. One such contribution is the assumption that the wave conditions at BD1 and BD2 are the same as those at adjacent transects, even though the coastline angle changes. Secondly, the presence of reefs in the nearshore zone may cause wave refraction between the 10 m depth contour and the location of wave breaking that is not taken into account in the Larson et al. (2010) wave refraction approach used here. Finally, the assumption of no sediment fluxes at the boundaries forces the longshore model to conserve sediment, although the sediment budget is not necessarily strictly closed if sediment either bypasses the rocky outcrop at the southern end of the beach or is gained or lost at the lagoon mouth at the northern end of beach.

Finally, biases in the wave height have significantly smaller impacts on the resultant shoreline changes than biases in the wave angle (Fig. 7b,e), causing shoreline position changes on the order of 3 m for wave height biases as large as 30%. When generating wave conditions from wind-forced wave models, Komen et al. (1996) estimated that a 10% error in the surface wind speed can cause a 10–20% error in the wave height. Thus, similar to George et al. (2019), the range of wave height bias errors β' tested in this study ranged from 5% to 30%, representing a potentially common range of errors encountered at sites with limited wave data. However, these biases are significantly larger than the expected values at Narrabeen beach, where Turner et al. (2016) estimated wave height biases on the order of only 3-4%.

6.5 Comparison of corrected and SWAN model breaking wave angles

To investigate the cause of the wave bias and the validity of the wave angle corrections $\tau_{n+1/2}$ proposed here, the corrected mean wave direction at the breaking point $\tilde{\alpha}_{b,n+1/2}$ obtained in this analysis (after using the Larson et al. (2010) method to propagate $\tilde{\alpha}_{w,n+1/2}$ to the breaking point) is compared to the breaking wave direction derived interdependently from a high resolution SWAN model (Harley et al. 2011) (Fig. 10b). These data are produced using a look-up table similar to that described in Turner et al. (2016), after extending it from producing wave conditions at 10 m water depth to the break point (thereby taking into account the additional refraction caused by nearshore reefs). The SWAN simulations were run using a single directional spreading value (30°) and were calibrated using nearshore wave data, showing a high correlation for the wave height and a slightly lower correlation for the wave direction (approximately 0.9 and 0.7, respectively Turner et al. 2016). While the SWAN model succeeds overall in reproducing the nearshore wave conditions, a deterministic wave model such as XBeach may be able to reproduce better the breaking wave conditions for this complex bathymetry. Before comparing the wave angles at the breaking point, it is important to note that the refraction calculated by the Larson et al. (2010) method between 10 m depth and the breaking point is small, ranging from 0° in the north to approximately -7° in the south (Fig. 10a). The estimated refraction effects are even smaller for the corrected wave angles $\tilde{\alpha}_{w,n+1/2}$ since on average the difference between the offshore wave angle and the coastline orientation decreased.

The comparison of the optimal breaking wave angles obtained in this analysis ($\tilde{\alpha}_b$) with the SWAN breaking wave angle ($\alpha_{b,SWAN}$) shows good overall agreement (Fig. 10b), supporting the hypothesis that the errors generated by the one-line model are caused by biases in the input wave angle. The corrected breaking wave angles are in general close to the SWAN breaking wave angles. The largest differences are observed at PF1, which is close to the model boundary, and PF6, where the wave angle bias is overestimated in comparison to the SWAN model look-up table. The largest change (nearly 20°) between the original (α_b) and corrected ($\tilde{\alpha}_b$) wave angle time series occurred at PF8, where $\tilde{\alpha}_b$ now agrees well with $\alpha_{b,SWAN}$. It is assumed that the optimal wave angle bias at this location primarily corrects for the underestimation of local wave refraction caused by a nearshore reef.

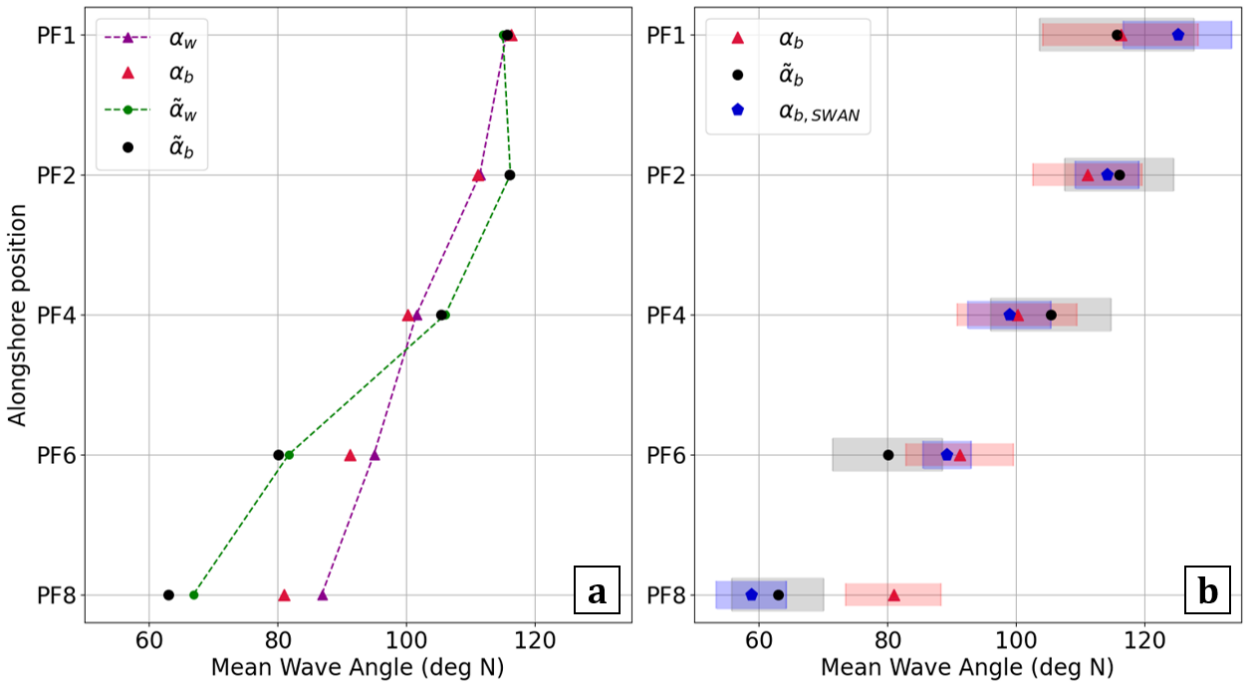

Figure 10: Temporal mean input and breaking wave angles: (a) Comparison between the mean original α_w (purple triangles) and corrected $\tilde{\alpha}_w$ (green points) 10 m depth wave angles, and the original α_b (red triangles) and corrected $\tilde{\alpha}_b$ (black points) breaking wave angles propagated using the Larson et al. (2010) method. (b) Comparison between the mean original (red triangles), corrected (black points), and SWAN (blue points) breaking wave angles, where the shaded zones indicate the standard deviation.

6.6 Wave data uncertainties

Morphological evolution models are forced with wave conditions derived from observations (e.g. wave buoys) and model outputs (e.g. spectral wave models). This study shows the sensitivity of a one-line longshore model to errors in the input wave direction, which then propagate through the modeling chain to cause errors in the predicted morphological changes. This is an important result because it is well known that the wave direction is difficult to estimate accurately with spectral wave models, often showing large uncertainties (e.g. Ardhuin & Roland 2013, Cavaleri et al. 2018), and that wave buoy observations also have errors in measured wave angles (e.g. Barstow et al. 2005). Even if the input wave conditions are known with high accuracy from one of these sources, wave conditions are often obtained at an offshore location and then must be propagated to the breaking point to be input in the one-line model flux calculation. Therefore, at the breaking point, it is often difficult to have highly accurate knowledge of the wave conditions, and in particular the incident wave angle, in particular in areas where refraction over complex bathymetry may be significant and not necessarily represented well when using simple wave transformation approaches. An additional limitation in one-line longshore models is that bulk wave parameters are used to force the model, and thus the potential complexity of the full-spectra is neglected (e.g. existence of secondary swells, bimodal spectra, or high wave angle spreading).

This study highlights the importance of propagating accurately offshore wave conditions to the nearshore zone to force morphological evolution models. One-line longshore models are particularly sensitive to the input wave angle, and even more so, to alongshore gradients in the input wave angle. In addition, this work also demonstrates that having high-quality estimates of nearshore wave conditions at 10 m depth may not be sufficient in particular cases where there is significant refraction shoreward of this location up to the breaking point (e.g. for embayed beach or beaches with complex nearshore bathymetry such as Narrabeen). However, it is not common to have access to high-quality, high-resolution, long-term estimates of wave conditions at the wave breaking point due to the high computational costs associated with nearshore wave propagation models. This emphasizes the need for further developments in nearshore in situ hydrodynamics monitoring and accurate and efficient nearshore wave propagation models, as well as the necessity to take into account uncertainties in morphological evolution studies.

7 Conclusions

In this study, the sensitivity of a commonly used one-line longshore sediment transport model to the input wave angle is evaluated using a statistical approach. The study is carried out at Narrabeen beach for the 10-year period from 2005 to 2015, where the model, forced with an available dataset of wave conditions at the 10 m depth contour, simulated a change in the shoreline planform orientation that was different from that of the observations. The objective of the current work is to study the source of this error and to understand the sensitivity of the one-line longshore model to the input wave angle by using a Monte Carlo approach to correct the wave angle time series by adding randomly generated biases (spatially variable but temporally constant). The model sensitivity is further quantified by comparing the simulated shoreline position at the end of the 10-year period to the observations and to the reference test case corresponding to the optimal wave bias correction.

The results of the first analysis show that by correcting the wave angle time series with the optimal set of biases (in the range of -20° to 5°), the simulated shoreline planform orientation agrees well with the observations. The shoreline position error distributions resulting from the wave angle and wave height bias sensitivity analyses demonstrate that the one-line longshore model is highly sensitive to biases in the wave angle. For example, the standard deviation of the shoreline position errors increases by approximately 5 m for a 1° increase in the wave direction bias, but by less than 1 m for a 10% bias in the wave height.

The breaking wave angles obtained from the optimal corrected biases in this study generally agree well with the breaking wave angles obtained by propagating offshore wave conditions using the SWAN model. This comparison also demonstrated that the corrections to the mean wave direction are coherent with wave refraction processes in the nearshore zone, which are not taken into account in simple wave transformation models often used to estimate wave breaking conditions. Thus, the methodology presented in this paper is able to compensate for the lack of accurate breaking wave direction data by using available morphological observations.

Finally, this study highlights the need for high quality estimates of breaking wave conditions, and in particular, the wave breaking direction and its alongshore gradients, in longshore sediment transport models. Even when nearshore (e.g. 10 m depth) wave conditions are known, simple propagation methods like the approach of Larson et al. (2010) should be used with caution in areas with complex bathymetry, and the uncertainties associated with these simple modeling approaches should be evaluated.

Acknowledgements

Teddy Chataigner's thesis is financed by the *Agence de l'Innovation de Défense* (AID) program of the *Direction Générale de l'Armement* (DGA), the Cerema, and the Ecole des Ponts.

References

Anderson, D., Ruggiero, P., Antolínez, J. A. A., Méndez, F. J. & Allan, J. (2018), 'A climate index optimized for longshore sediment transport reveals interannual and multidecadal littoral cell rotations', *Journal of Geophysical Research: Earth Surface* **123**(8), 1958–1981.

Antolínez, J. A. A., Méndez, F. J., Anderson, D., Ruggiero, P. & Kaminsky, G. M. (2019), 'Predicting climate-driven coastlines with a simple and efficient multiscale model', *Journal of Geophysical Research: Earth Surface* **124**(6), 1596–1624.

Ardhuin, F. & Roland, A. (2013), 'The development of spectral wave models: Coastal and coupled aspects', *Proceedings of Coastal Dynamics 2013: 7th International Conference on Coastal Dynamics* .

Ashton, A. D. & Murray, A. B. (2006), 'High-angle wave instability and emergent shoreline shapes: 1. modeling of sand waves, flying spits, and capes', *Journal of Geophysical Research: Earth Surface* **111**(F4).

Athanasiou, P., Van Dongeren, A. R., Giardino, A., Vousdoukas, M. I., Ranasinghe, R. & Kwadijk, J. (2020), 'Uncertainties in projections of sandy beach erosion due to sea level rise: an analysis at the european scale', *Sci Rep* **10**.

Barstow, S. F., Bidlot, J.-R., Caires, S., Donelan, M. A., Drennan, W. M., Dupuis, H., Graber, H. C., Green, J. J., Gronlie, O., Guérin, C., Gurgel, K.-W., Günther, H., Hauser, D., Hayes, K., Hessner, K., Hoja, D., Icard, D., Kahma, K. K., Keller, W. C., Krogstad, H. E., Lefevre, J.-M., Lehner, S., Magnusson, A. K., Monbaliu, J., Nieto Borge, J. C., Pettersson, H., Plant, W. J., Quentin, C. G., Reichert, K., Reistad,

M., Rosenthal, W., Saetra, O., Schulz-Stellenfleth, J., Walsh, E. J., Weill, A., Wolf, J., Wright, C. W. & Wyatt, L. R. (2005), *Measuring and Analysing the directional spectrum of ocean waves*, COST 714; EUR 21367, COST Office.

Bayram, A., Larson, M., Miller, H. C. & Kraus, N. C. (2001), Cross-shore distribution of longshore sediment transport:comparison between predictive formulas and field measurements, *in* 'Coastal Engineering 2000', American Society of Civil Engineers, pp. 3114–3127.

Bergillos, R., López-Ruiz, A., Principal-Gómez, D. & Ortega-Sánchez, M. (2018), 'An integrated methodology to forecast the efficiency of nourishment strategies in eroding deltas', *Sci Total Environ* **613-614**, 1175–1184.

Bouchette, F., Manna, M., Montalvo, P., Nutz, A., Schuster, M. & Ghienne, J.-F. (2014), 'Growth of cuspate spits', *Journal of Coastal Research* pp. 47–52.

Cavaleri, L., Abdalla, S., Benetazzo, A., Bertotti, L., Bidlot, J., Breivik, O., Carniel, S., Jensen, R., Portilla-Yandun, J., Rogers, W., Roland, A., Sanchez-Arcilla, A., Smith, J., Staneva, J., Toledo, Y., Vledder, G. & Westhuysen, A. (2018), 'Wave modelling in coastal and inner seas', *Progress in Oceanography* **167**.

D'Anna, M., Idier, D., Castelle, B., Le Cozannet, G., Rohmer, J. & Robinet, A. (2020), 'Impact of model free parameters and sea-level rise uncertainties on 20-years shoreline hindcast: the case of Truc Vert beach (SW France)', *Earth Surface Processes and Landforms* **45**(8), 1895–1907.

Davidson, M. A., Turner, I. L., Splinter, K. D. & Harley, M. D. (2017), 'Annual prediction of shoreline erosion and subsequent recovery', *Coastal Engineering* **130**, 14 – 25.

Davidson, M., Splinter, K. & Turner, I. (2013), 'A simple equilibrium model for predicting shoreline change', *Coastal Engineering* **73**, 191–202.

Delft Hydraulics, W. (1994), *UNIBEST, A software suite for the simulation of sediment transport processes and related morphodynamics of beach profiles and coastline evolution.*

Durrant, T., Greenslade, D., Hemer, M. & Trenham, C. (2014), A global wave hindcast focussed on the central and south pacific, Technical report, CAWCR Technical Report No. 070.

D'Anna, M., Castelle, B., Idier, D., Rohmer, J., Le Cozannet, G., Thieblemont, R. & Bricheno, L. (2021), 'Uncertainties in shoreline projections to 2100 at truc vert beach (france): Role of sea-level rise and equilibrium model assumptions', *Journal of Geophysical Research: Earth Surface* .

French, J., Payo, A., Murray, B., Orford, J., Eliot, M. & Cowell, P. (2016), 'Appropriate complexity for the prediction of coastal and estuarine geomorphic behaviour at decadal to centennial scales', *Geomorphology* **256**, 3 – 16.

George, J., Sanil Kumar, V., Victor, G. & Gowthaman, R. (2019), 'Variability of the local wave regime and the wave-induced sediment transport along the ganpatipule coast, eastern arabian sea', *Regional Studies in Marine Science* **31**.

Hallermeier, R. J. (1983), 'Sand transport limits in coastal structure design', *Proceedings, Coastal Structures '83, American Society of Civil Engineers* pp. pp. 703–716.

Hanson, H. (1989), 'Genesis: A generalized shoreline change numerical model', *Journal of Coastal Research* **5**(1), 1–27.

Harley, M., Andriolo, U., Armaroli, C. & Ciavola, P. (2014), 'Shoreline rotation and response to nourishment of a gravel embayed beach using a low-cost video monitoring technique: San michele-sassi neri, central italy', *Journal of Coastal Conservation* **18**, 551–565.

Harley, M. D., Turner, I. L. & Short, A. D. (2015), 'New insights into embayed beach rotation: The importance of wave exposure and cross-shore processes', *Journal of Geophysical Research: Earth Surface* **120**(8), 1470–1484.

Harley, M. D., Turner, I. L., Short, A. D. & Ranasinghe, R. (2010), 'Interannual variability and controls of the sydney wave climate', *International Journal of Climatology* **30**(9), 1322–1335.

Harley, M. D., Turner, I. L., Short, A. D. & Ranasinghe, R. (2011), 'A reevaluation of coastal embayment rotation: The dominance of cross-shore versus alongshore sediment transport processes, collaroy-narrabeen beach, southeast australia', *Journal of Geophysical Research: Earth Surface* **116**(F4).

Jaramillo, C., González, M., Medina, R. & Turki, I. (2021), 'An equilibrium-based shoreline rotation model', *Coastal Engineering* **163**, 103789.

Kamphuis, J., Davies, M., Nairn, R. & Sayao, O. (1986), 'Calculation of littoral sand transport rate', *Coastal Engineering* **10**(1), 1–21.

Komen, G. J., Cavaleri, L., Donelan, M., Hasselmann, K., Hasselmann, S. & Janssen, P. A. E. M. (1996), *Dynamics and Modelling of Ocean Waves*.

Kroon, A., De Schipper, M., Gelder, P. & Aarninkhof, S. (2020), 'Ranking uncertainty: Wave climate variability versus model uncertainty in probabilistic assessment of coastline change', *Coastal Engineering* **158**, 103673.

Larson, M., Hanson, H. & Kraus, N. C. (1997), 'Analytical solutions of one-line model for shoreline change near coastal structures', *Journal of Waterway, Port, Coastal, and Ocean Engineering* **123**(4), 180–191.

Larson, M., Hoan, L. & Hanson, H. (2010), 'Direct formula to compute wave height and angle at incipient breaking', *Journal of Waterway Port Coastal and Ocean Engineering* **136**.

Le Cozannet, G., Bulteau, T., Castelle, B., Ranasinghe, R., Wöppelmann, G., Rohmer, J., Bernon, N., Idier, D., Louisor, J. & Salas-Y-Mélia, D. (2019), 'Quantifying uncertainties of sandy shoreline change projections as sea level rises', *Scientific reports* **9**(1), 42.

Miller, J. K. & Dean, R. G. (2004), 'A simple new shoreline change model', *Coastal Engineering* **51**(7), 531–556.

Montaño, J., Coco, G., Antolínez, J. A. A., Beuzen, T., Bryan, K. R., Cagigal, L., Castelle, B., Davidson, M. A., Goldstein, E. B., Ibaceta, R., Idier, D., Ludka, B. C., Masoud-Ansari, S., Méndez, F. J., Murray, A. B., Plant, N. G., Ratliff, K. M., Robinet, A., Rueda, A., Sénéchal, N., Simmons, J. A., Splinter, K. D., Stephens, S., Townend, I., Vitousek, S. & Vos, K. (2020), 'Blind testing of shoreline evolution models', *Scientific Reports* **10**.

Murray, A. B. (2007), 'Reducing model complexity for explanation and prediction', *Geomorphology* **90**(3), 178 – 191. Reduced-Complexity Geomorphological Modelling for River and Catchment Management.

Pelnard-Considére, R. (1956), 'Essai de théorie de l'évolution des formes de rivages en plages de sable et de galets', *La Houille Blanche* pp. 289–301.

Pilkey, O. & Cooper, A. (2002), 'Longshore transport volumes: A critical view', *Journal of Coastal Research* **36**, 572–580.

Ranasinghe R., Callaghan D., R. D. (2013), 'Does a more sophisticated storm erosion model improve probabilistic erosion estimates?', *Coastal Dynamic* .

Reeve, D., Pedrozo-Acuña, A. & Spivack, M. (2014), 'Beach memory and ensemble prediction of shoreline evolution near a groyne', *Coastal Engineering* **86**, 77–87.

Robinet, A., Castelle, B., Idier, D., Harley, M. & Splinter, K. (2020), 'Controls of local geology and cross-shore/longshore processes on embayed beach shoreline variability', *Marine Geology* **422**, 106118.

Robinet, A., Idier, D., Castelle, B. & Marieu, V. (2018), 'A reduced-complexity shoreline change model combining longshore and cross-shore processes: The lx-shore model', *Environmental Modelling & Software* **109**, 1 – 16.

Roelvink, D., Reniers, A., van Dongeren, A., van Thiel de Vries, J., McCall, R. & Lescinski, J. (2009), 'Modelling storm impacts on beaches, dunes and barrier islands', *Coastal Engineering* **56**(11), 1133 – 1152.

Roelvink, J. & Banning, G. (1995), 'Design and development of delft3d and application to coastal morphodynamics', *Oceanographic Literature Review* **11**, 925.

Ruggiero, P., Buijsman, M., Kaminsky, G. & Gelfenbaum, G. (2010), 'Modeling the effects of wave climate and sediment supply variability on large-scale shoreline change', *Marine Geology* **273**, 127–140.

Safak, I., List, J., Warner, J. & Kumar, N. (2017), 'Observations and 3D hydrodynamics-based modeling of decadal-scale shoreline change along the Outer Banks, North Carolina', *Coastal Engineering* **120**, 78 – 92.

Splinter, K. D., Turner, I. L., Davidson, M. A., Barnard, P., Castelle, B. & Oltman-Shay, J. (2014), 'A generalized equilibrium model for predicting daily to interannual shoreline response', *Journal of Geophysical Research: Earth Surface* **119**(9), 1936–1958.

Toimil, A., Camus, P., Losada, I., Le Cozannet, G., Nicholls, R., Idier, D. & Maspataud, A. (2020), 'Climate change-driven coastal erosion modelling in temperate sandy beaches: Methods and uncertainty treatment', *Earth-Science Reviews* **202**, 103110.

Tran, Y. H. & Barthélemy, E. (2020), 'Combined longshore and cross-shore shoreline model for closed embayed beaches', *Coastal Engineering* **158**, 103692.

Turki, I., Medina, R., Coco, G. & González, M. (2013), 'An equilibrium model to predict shoreline rotation of pocket beaches', *Marine Geology* **346**, 220–232.

Turner, I., Harley, M., Short, A., Simmons, J., Bracs, M., Phillips, M. & Splinter, K. (2016), 'A multi-decade dataset of monthly beach profile surveys and inshore wave forcing at narrabeen, australia', *Scientific data* **3**.

USACE (1984), Shore Protection Manual, Technical report, U.S. Army Corps of Engineers, Vicksburg, Mississippi.

Valiente, N. G., Masselink, G., Scott, T., Conley, D. & McCarroll, R. J. (2019), 'Role of waves and tides on depth of closure and potential for headland bypassing', *Marine Geology* **407**, 60–75.

Vitousek, S., Barnard, P. L., Limber, P., Erikson, L. & Cole, B. (2017), 'A model integrating longshore and cross-shore processes for predicting long-term shoreline response to climate change', *Journal of Geophysical Research: Earth Surface* **122**(4), 782–806.

Wang, B. & Reeve, D. (2010), 'Probabilistic modelling of long-term beach evolution near segmented shore-parallel breakwaters', *Coastal Engineering* **57**(8), 732–744.

Warren, I. & Bach, H. (1992), 'Mike 21: a modelling system for estuaries, coastal waters and seas', *Environmental Software* **7**(4), 229–240. 3rd International Software Exhibition for Environmental Science and Engineering.

Wright, L. D. & Short, A. D. (1984), 'Morphodynamic variability of surf zones and beaches: A synthesis', *Mar. Geol.* **56**, 93–118.

Yates, M. L., Guza, R. T. & O'Reilly, W. C. (2009), 'Equilibrium shoreline response: Observations and modeling', *J. Geophys. Res.* **114**(C09014).